Available online at www.sciencedirect.com
ScienceDirect
Magnetic Resonance Imaging 24 (2006) 1229–1240
MAGNETIC RESONANCE IMAGING

Slice profile optimization in arterial spin labeling using presaturation and optimized RF pulses

David Alberg Holm[a,b,*], Karam Sidaros[a]

[a]Danish Research Centre for Magnetic Resonance, Copenhagen University Hospital, 2650 Hvidovre, Denmark
[b]Informatics and Mathematical Modelling, Technical University of Denmark, 2800 Lyngby, Denmark

Received 4 November 2005; accepted 2 July 2006

Abstract

Objective: An important source of error in arterial spin labeling (ASL) is incomplete static tissue subtraction due to imperfect slice profiles. This effect can be reduced by saturating the spins in the imaging area prior to labeling. In this study, the use of optimized presaturation is compared with the use of optimized RF pulses for minimizing this error.

Materials and Methods: Different methods for optimizing presaturation were simulated by numerical solution of the Bloch equation. Presaturation was optimized by changing the number of presaturation pulses, their position in the pulse sequence and the area of the crusher gradients following each saturation pulse. It was also investigated whether the use of optimized presaturation could reduce the tag gap needed to ensure complete static tissue subtraction. Simulation results were verified using phantom and in vivo studies at 3T.

Results: In proximal inversion with control for off-resonance effects, optimized presaturation could reduce the necessary tag gap to 15% of the imaging slab for experiments using standard RF pulses, while c-FOCI RF pulses could reduce it to 11%. In flow-sensitive alternating inversion recovery, a single presaturation pulse could reduce the inversion width to 122% of the imaging slab and neither multiple presaturation pulses nor optimized RF pulses could reduce it further.

Conclusion: Optimized presaturation can reduce the necessary inversion width to the same level as if using optimized RF pulses and can, therefore, be used to optimize ASL sensitivity. Furthermore, optimized presaturation can reduce the B_1-dependent sensitivity in static tissue subtraction.

Keywords: Arterial spin labeling; Perfusion measurement; Static tissue subtraction; Presaturation

1. Introduction

Arterial spin labeling (ASL) is becoming an established method for performing noninvasive perfusion measurements in vivo. There are numerous ASL techniques, and most approaches acquire two images: a tag image in which arterial spins proximal to the area of interest are tagged or labeled by inversion and a control image where the arterial spins are not inverted. In one approach, proximal inversion with control for off-resonance effects (PICORE) [1], the tag image is acquired after inverting the spins in a slab proximal to imaging slab. The control experiment is performed in the same way, but here, the slice-select gradient is turned off during the inversion pulse, making it off resonance. In flow-sensitive alternating inversion recovery (FAIR) [2], the tag experiment is performed by nonselectively inverting everything in the coil. The control experiment is performed by selectively inverting the tissue and blood in the imaging slab [3].

The difference between the tag and control images is perfusion weighted and is on the order of 1% of the equilibrium magnetization. Even small systematic differences between the images can, therefore, lead to significant errors in the estimation of the perfusion.

Frank et al. have shown that a large amount of error is due to imperfect slice profiles [4]. Nonideal inversion pulses can affect the spins in the imaging area, resulting in a systematic difference between the tag and control image that is not related to perfusion [4,5]. The effect of imperfect slice profiles can be reduced by introducing a gap (tag gap) between the inversion and imaging slabs in PICORE or by increasing the width of the slice-selective inversion slab in

* Corresponding author. Hvidovre Hospital, afd 340, DK-2650 Hvidovre, Denmark. Tel.: +45 36 32 29 76; fax: +45 36 47 03 02.
E-mail address: davidh@drcmr.dk (D.A. Holm).

0730-725X/$ – see front matter © 2006 Elsevier Inc. All rights reserved.
doi:10.1016/j.mri.2006.07.011

Table 1
Position of saturation pulses in the sequence and crusher gradient areas (in mT/m · ms) used in Simulation 1

Simulation	RF pulse order	First crusher	Second crusher
1A, 2 presats	90°–90°–180°	0–80	0–80
1B, presat/postsat	90°–180°–90°	0–80	0–160
1C, 2 postsats	180°–90°–90°	0–160	0–80

FAIR. However, introducing such a gap results in an increased transit delay (the delay from the time of tagging the arterial blood until it reaches the tissue of interest). During this transit delay, the tagged bolus of blood undergoes T_1 relaxation, which reduces the perfusion weighting [6].

Previous studies have focused on the use of optimized RF pulses for inversion in order to reduce the minimum tag gap needed to ensure complete static tissue subtraction [4–7]. An alternative is to use presaturation, where the magnetization in the imaging area is saturated immediately before tagging arterial blood, thereby reducing non-perfusion-related differences between the tag and control images. The efficacy of the presaturation can be increased by using multiple presaturation pulses. However, previous experiments have shown that increasing the number of presaturation pulses may also lead to a large systematic difference (referred to as an offset) between the tag and control images [8]. This offset is caused by the interactions between RF pulses: for example, remaining transverse magnetization after one RF pulse can be rotated into the longitudinal direction by the following RF pulse and affect the resulting magnetization profile.

In this study, the effect of changing the position of the presaturation pulses in the sequence, their number and the size of the crusher gradient following each RF pulse is investigated. Furthermore, the B_1 sensitivity of each approach is investigated. Results are compared with the effect of using optimized inversion pulses.

2. Methods

This study includes simulations as well as phantom and in vivo experiments. As the number of parameters that can be investigated in vivo is restricted by the total scanning time, simulations were run to explore which parameters were likely to have an effect on the minimum tag gap. The results were then verified in phantoms, and finally, the use of optimized presaturation was tested in vivo to see if it could reduce the minimum tag gap, hence increasing the signal in ASL measurements.

Saturation pulses placed immediately before the inversion pulse will, in the following, be referred to as *presat* pulses, while saturation pulses placed immediately after the inversion pulse will be referred to as *postsat* pulses. The width of the saturation slab was the imaging slab plus the tag gap, which centers the edge of the saturation slab between the edges of the imaging and inversion slabs.

The efficacy of presaturation was tested with different positions of the presaturation pulses in the sequence, and the results were compared with simulations using optimized RF pulses.

2.1. Simulations

Static tissue subtraction can be improved by using either presaturation or optimized RF pulses. Simulations can be used to investigate the effects of the order of presaturation pulses (Simulation 1), to show differences between different RF pulses (Simulation 2), to show if optimized presaturation can reduce the necessary tag gap (Simulation 3), to compare optimized presaturation to the use of optimized RF pulses (Simulation 4) and to investigate the B_1 sensitivity of the different presaturation strategies (Simulation 5).

Simulation of the effect of the RF pulses was performed by numerical solution of the Bloch equation in Matlab 6.5 (The MathWorks Inc., Natick, MA, USA). The magnetization profile across the slice after the application of the RF pulses was calculated, and the integral of the transverse magnetization over the profile was used as an estimate of the signal that would be measured in an ASL experiment. The magnetization was assumed to be in equilibrium before each acquisition; that is, a long TR was assumed.

All simulations were carried out using five 5-mm slices with an interslice gap of 10%, giving an imaging slab of 27 mm. These parameters were chosen as they are often used in vivo.

Although the simulations were done for specific values of slice thickness, inversion slab thickness and so on, the problem is highly scalable and generalizable. In FAIR, all the RF pulses are centered on the imaging slab, and multiplying

Table 2
RF pulses and parameters

Abbreviation	Saturation pulse	Inversion pulse	Imaging pulse
2A, Sinc/HS	Hanning filtered sinc pulses (T=12.8 ms, BW=1250 Hz)	HS (T=15 ms, μ=10, β=800 Hz)	Hanning filtered sinc pulse (T=5.12 ms, BW=2031 Hz)
2B, SLR/HS	Hamming filtered SLR pulse (90° MP, T=10.24 ms, BW=2000 Hz, PBR 0.04%, RBR 0.1%)	HS (T=15 ms, μ=10, β=800 Hz)	Hamming filtered SLR pulse (90° REF, T=5.12 ms, BW=2000 Hz, PBR 0.04%, RBR 0.1%)
2C, Sinc/FOCI	Hanning filtered sinc pulses (T=12.8 ms, BW=1250 Hz)	FOCI (P=10, T=15 ms, μ=10, β=800 Hz)	Hanning filtered sinc pulse (T=5.12 ms, BW=2031 Hz)

MP, maximum phase; REF, refocused; PBR, passband ripple; RBR, rejection band ripple.
FOCI, c-shape frequency offset corrected inversion [14]; SLR, Shinnar Le Roux [15,16]; T, pulse duration; P, FOCI multiplication factor.

Table 3
Optimal and suboptimal crusher gradient areas for PICORE selected from Simulation 1 (in mT/m · ms)

Simulation	RF pulse order	Optimal crusher areas			Suboptimal crusher areas		
		First	Second	Third	First	Second	Third
3A, no presats	180°	82.8	–	–	–	–	–
3B, 1 presat	90°–180°	41.4	82.8	–	–	–	–
3C, 2 presats	90°–90°–180°	17.8	50.1	82.8	43.1	43.1	82.8
3D/, presat/postsat	90°–180°–90°	43.1	82.8	41.4	20.0	28.0	41.4
3E, 2 postsats	180°–90°–90°	80.0	43.1	41.4	43.1	43.1	41.4

slice thickness and saturation and inversion slab thicknesses by a constant does not change the geometry. This is done by reducing the gradients during the RF pulses, and one must reduce the crusher gradients by the same factor. Changing the number of slices, in principle, changes the geometry of the problem, but as long as the slice thickness is much smaller than the imaging slab thickness, this is not expected to play a major role in the degree of static tissue subtraction. For PICORE, the results are slightly less generalizable since the inversion slab is adjacent to the imaging slab. However, the problem is perfectly scalable by changing the slice thickness, tag gap, inversion slab thickness and crusher gradients by the same factor. Changing the number of slices without changing slice thickness, on the other hand, changes the imaging and saturation slab thicknesses, which changes the interaction between the inversion and saturation slab profiles. This could be partly overcome by adjusting the tag gap and inversion slab thickness by the same factor as the number of slices.

The following five simulations were performed to explore the dependence of the degree of static tissue subtraction on specific presaturation parameters, including pulse position in the sequence and crusher gradients as well as the choice of RF pulses.

2.1.1. Simulation 1: presaturation pulse order

The purpose of this simulation was to explore the effect of the area of the crusher gradients that follow the presaturation and inversion pulses, as well as to study the effect of changing the position of the presaturation pulses in the sequence.

Two presaturation pulses were used and were placed immediately before inversion (two presats), immediately after inversion (two postsats) or one before and one after inversion (prestat/postsat; see Table 1). The crusher gradient after the last RF pulse is not important since any remaining transverse magnetization naturally decays due to T_2 relaxation during the inversion time TI, where TI$>T_2$.

The simulation was run for PICORE with a tag gap of 18.5% of the imaging slab (5 mm) and for FAIR with an inversion slab that was 137% of the imaging slab (37 mm). The RF pulses used for presaturation were Hanning filtered sinc pulses [12.8 ms, bandwidth (BW)=1250 Hz]; the inversion pulse was a hyperbolic secant (HS) pulse (15 ms, μ=10, β=800 Hz [9]), and the imaging pulse was a Hanning filtered sinc pulse (5.12 ms, BW=2031 Hz).

2.1.2. Simulation 2: comparison with optimized RF pulses

The purpose of this simulation was to investigate how the choice of RF pulses used for inversion, saturation and imaging affects the offset between the signals in the tag and control experiments. Simulation 1 was repeated using different RF pulses. The RF pulses used are listed in Table 2. The Shinnar le Roux (SLR) pulses were designed using the program Matpulse [10] with the parameters listed in the table.

2.1.3. Simulation 3: effect of optimal presaturation on the minimal tag gap

This simulation was run to investigate if the use of optimized presaturation could reduce the minimal tag gap required to ensure complete static tissue subtraction. Simulations were performed, stepping the tag gap from 0% to 74% of the imaging slab (0 to 20 mm) for PICORE and stepping the inversion/imaging slab ratio from 100% to 248% (27–67 mm) for FAIR experiments. Crusher gradient areas were selected from Simulation 1 in the regions showing the lowest offset. The RF pulses used were sinc/HS as shown in Table 2 (Simulation 2A). The used crusher areas are listed in Tables 3 and 4 under optimal crusher areas.

Table 4
Optimal and suboptimal crusher gradient areas for FAIR selected from Simulation 1 (in mT/m · ms)

Simulation	RF pulse order	Optimal crusher areas			Suboptimal crusher areas		
		First	Second	Third	First	Second	Third
4A, no presats	180°	82.8	–	–	–	–	–
4B, 1 presat	90°–180°	41.4	82.8	–	–	–	–
4C, 2 presats	90°–90°–180°	59.6	24.8	82.8	43.1	50.1	82.8
4D, presat/postsat	90°–180°–90°	35.2	99.4	41.4	21.9	19.9	41.4
4E, 2 postsats	180°–90°–90°	99.4	35.2	41.4	19.9	31.9	41.4

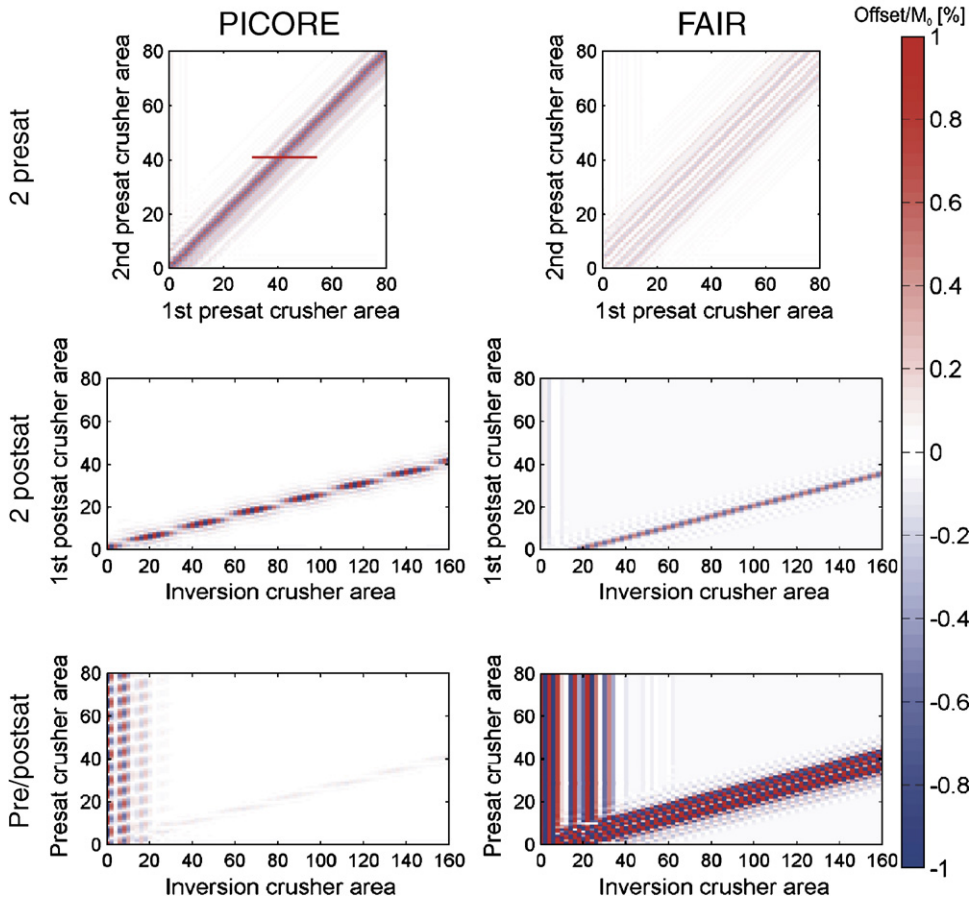

Fig. 1. Presaturation pulse order. This figure shows the offset relative to M_0 obtained in Simulation 1 as a function of crusher gradient areas (mT/m • ms). The presaturation position is shown on the left, and the labeling method is shown at the top. The red line in the top left panel indicates the crushers used for validation in Phantom Experiment 1 (Fig. 6).

2.1.4. Simulation 4: effect of optimized RF pulses on the minimum tag gap

To further investigate the benefit of using optimized RF pulses combined with presaturation, we ran a simulation using different RF pulses for presaturation, inversion and imaging (Table 2) in FAIR and PICORE experiments with two presats. To highlight the difference between the different RF pulses, we ran the simulation using optimal and suboptimal crusher areas (Tables 3, Simulation 3C, and 4, Simulation 4C). The tag gap was stepped from 0% to 74% of the imaging slab (0–20 mm). The suboptimal crusher areas were selected from Simulation 1 in areas showing a large offset.

2.1.5. Simulation 5: effect of B_1 inhomogeneity

This simulation was run to investigate the dependence of the offset on B_1 (RF field) inhomogeneities, which are always present, especially at high field. Errors in the B_1 field, for example, due to dielectric effects, are expected to affect the slice profiles and flip angles of all the RF pulses used, thereby affecting the offset. The simulation was run using the RF pulses listed in Table 2 and optimal and suboptimal crusher areas in a PICORE experiment, with different ordering of the RF pulses (Table 3). The actual B_1 value was stepped from 80% to 120% of the nominal size. A tag gap of 18.5% of the imaging slab (5 mm) was used in the simulations.

2.2. Phantom and in vivo experiments

Phantom experiments were included to verify key results of the simulations. The phantom used did not include any flow, which means that the offset between the tag and control image can be directly compared with the simulated offset.

All phantom and in vivo experiments were performed on a Siemens Magnetom Trio 3-T scanner (Siemens, Erlangen, Germany). The RF pulses used in the ASL sequences were Hanning filtered sinc pulses for imaging and presaturation and HS pulses for inversion (Table 2, Simulation 2A). All experiments were acquired with a 64×64 matrix and single-shot GE-EPI readout.

2.2.1. Phantom Experiment 1

The purpose of the first phantom experiment was to verify the results of Simulation 1A. A cylindrical, homogenous, Gd-doped agarose gel phantom with T_1=1204 and T_2=90 ms was used. PICORE experiments with two presat pulses were performed while stepping the first

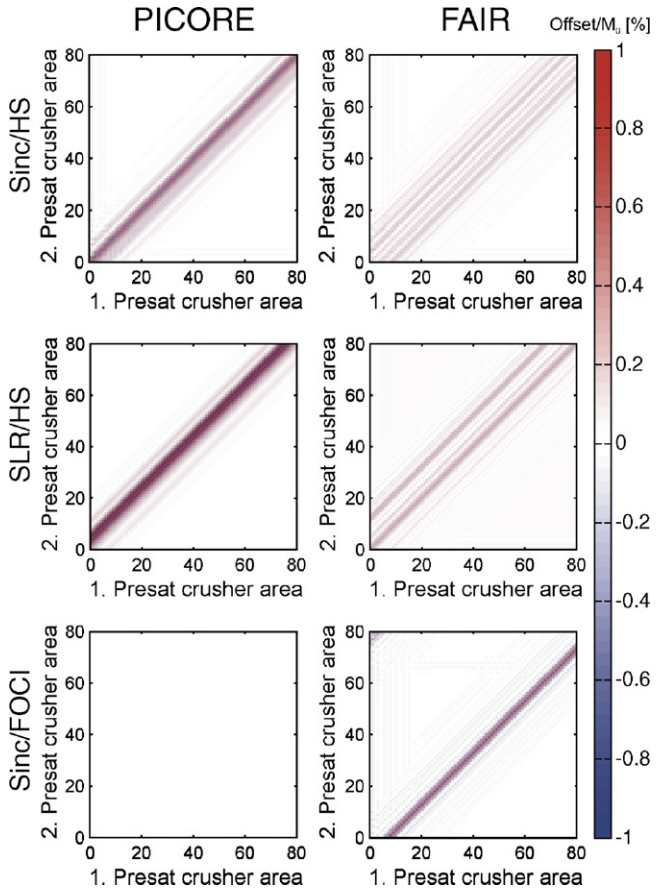

Fig. 2. Changing RF pulses. The calculated offset relative to M_0 as a function of the crusher gradient areas (mT/m • ms) following the presat pulses for the case of two presats and a tag gap of 18.5%. Three combinations of RF pulses were used in the simulations (Table 2). Note that the top two plots are the same as shown in Fig. 1.

presat crusher gradient area from 30 to 55 mT/m · ms. The second presat pulse had a fixed crusher gradient area of 41.41 mT/m · ms, while the inversion crusher area was 82.82 mT/m · ms.

The acquisition parameters for the PICORE experiments were 28 acquisitions (14 tag and 14 control), TE/TI/TR = 20/1000/5000 ms, five 5-mm slices with a 10% slice gap between slices. The tag gap was 18.5% of the imaging slab (5 mm). To correct for M_0 differences, we acquired an M_0 image with 11 acquisitions, 64×64 matrix, TE/TI/TR = 20/7500/8000 ms.

ASL magnetization difference (ΔM) images were calculated as the mean difference between the control and tag images. The ΔM images directly reveal the degree of static tissue subtraction since there is no perfusion in the phantom. Two regions of interest (ROIs) were defined by thresholding the M_0 images based on pixel intensity. The calculated ΔM values were averaged over the two ROIs and were normalized by the mean M_0 values (over the same ROIs).

One of the ROIs was selected centrally (n = 284 pixels) and the other peripherally (n = 284 pixels) to assess the effect of B_1 inhomogeneities on the measured offset, and the results were compared with the results from Simulation 5.

2.2.2. Phantom Experiment 2

The purpose of this experiment was to verify that optimized presaturation can reduce the minimum tag gap needed to assure complete static tissue subtraction, as well as to verify the results from Simulation 3A.

PICORE measurements were acquired with two presat pulses (crusher areas listed in Table 3), 22 acquisitions (11 tag and 11 control), TE/TI/TR = 20/1000/5000 ms, five 5-mm slices (10% slice gap). The tag gap was stepped from 0% to 74% of the imaging slab. An M_0 image was acquired as in Phantom Experiment 1.

2.2.3. In Vivo Experiment 1

In order to evaluate the effect of the choice of crusher gradients on the degree of static tissue subtraction in perfusion measurements in vivo, we scanned four subjects using PICORE (age range, 23–30 years; one female) and four subjects using FAIR (age range, 27–31 years; two females) with the values for pre- and postsat crusher gradient areas listed in Tables 3 and 4). Ten 5-mm slices with a 10% interslice gap (54.5 mm imaging slab) were acquired with 120 acquisitions (60 tag and 60 control images), TE/TI/TR = 20/1200/2000 ms, BW = 2604 Hz/pixel, and in addition, M_0 single-shot EPI images were acquired (one acquisition). To reduce effects of motion between experiments, we acquired M_0 images after each two acquisitions of ASL images. PICORE scans were performed with a tag gap of 9% and 18% of the imaging slab (5 and 10 mm). FAIR scans were performed with an inversion slab of 118% and 137% (64.5 and 74.5 mm). In order to estimate the magnitude of the offset in the measured perfusion images, we acquired a reference perfusion map, where no offset was expected. This map was acquired using two presats with optimal crusher values and a tag gap of 24% of the imaging slab for PICORE (13 mm) and an inversion slab of 148% of the imaging slab for FAIR (80.5 mm). The use of a large tag gap was designed to ensure that the effect of imperfect slice profiles was negligible.

ROIs were drawn for each subject in anterior and posterior gray and white matter in the most inferior three slices on the M_0 images. As there was some motion during the experiments, the ROIs were drawn conservatively to make sure that they only contained white or gray matter in all the acquired images. The acquired reference perfusion image was subtracted from all other perfusion images to give estimates of the offset, and the resulting images were normalized by the M_0 image acquired closest temporally to each perfusion image. The calculated offset was averaged for each ROI over subjects. The results were tested for significance using a Student's t test. The significance level used was 5%.

2.2.4. In Vivo Experiment 2

In order to estimate the minimum tag gap needed to ensure complete static tissue subtraction in vivo when using

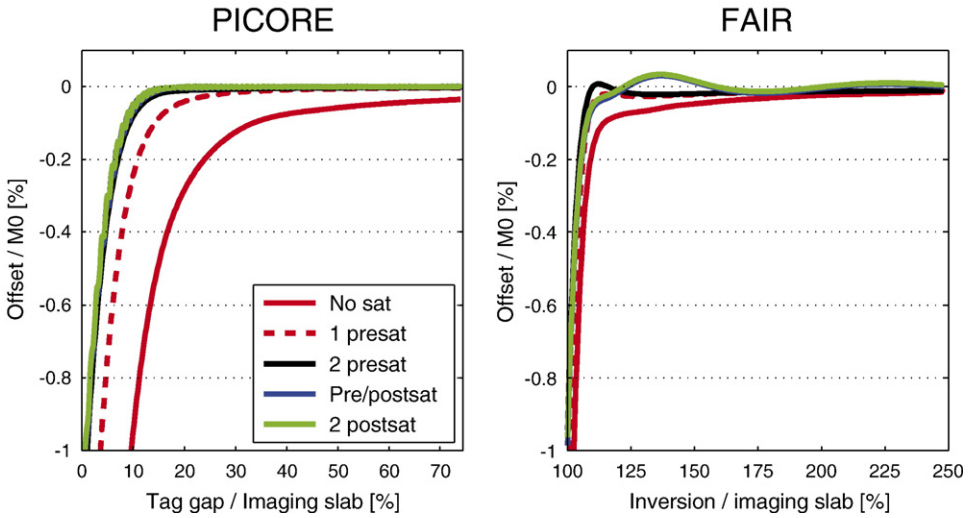

Fig. 3. Effect of changing the number/position of presaturation pulses. The calculated offset relative to M_0 as a function of gap for different number and placement of the presaturation pulses (see legend). The simulation results are plotted both for a PICORE experiment (A) and a FAIR experiment (B). The RF pulses used were HS/Sinc (Table 2, Simulation 2A). Crusher gradient areas are listed in Tables 3 and 4 (optimal).

optimal presaturation, we scanned four healthy volunteers (23–30 years; two females) using a PICORE sequence with two presats (using crusher areas listed in Table 3, Simulation 3C). The tag gap was stepped from 2% to 37% of the imaging slab (1–20 mm).

Ten 5-mm slices with an interslice gap of 10% (imaging slab, 54.5 mm) were acquired with 120 acquisitions (60 tag and 60 control images), TE/TI/TR=20/1000/2000 ms, BW=2604 Hz/pixel. In addition, M_0 single-shot EPI images were acquired (one acquisition). To reduce misregistration effects due to motion between experiments, we acquired M_0 images after each two acquisitions of ASL images.

ROIs were drawn as in Experiment 1. The acquired perfusion images were normalized using the M_0 image acquired closest temporally to each perfusion image. The perfusion data were averaged for each ROI over all subjects.

3. Results

All simulations and phantom and in vivo experiments were run with multiple slices; however, as the offset resulting from imperfect slice profiles is largest in the most proximal slice, mostly, results from that slice are described. In the in vivo PICORE experiments, the remaining slices showed similar but reduced offsets, while in FAIR, the offset was reduced in the middle slices and similar in the bottom and top slices.

3.1. Simulations

3.1.1. Simulation 1

The results of Simulation 1 with a tag gap of 18.5% are shown in Fig. 1. The figure shows that for two presats or presat/postsat, using equal crusher gradient areas after

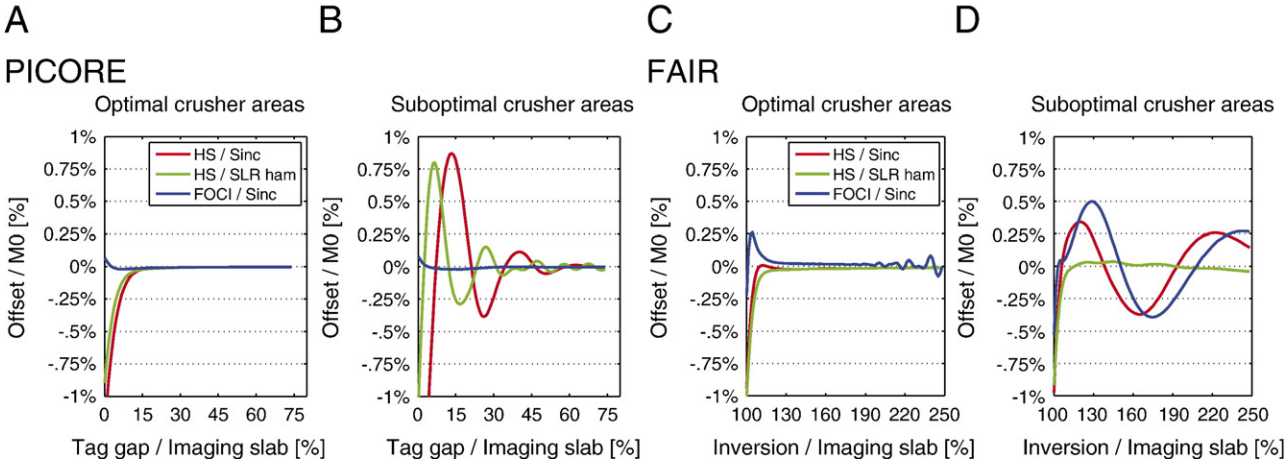

Fig. 4. Effect of using optimized RF pulses. The calculated offset relative to M_0 as a function of the gap for different RF pulses and crusher gradient combinations. Panels A and B are results for a PICORE experiment, while Panels C and D are those for a FAIR experiment. Crusher gradient areas are listed in Tables 3 (Simulation 3C) and 4 (Simulation 4C).

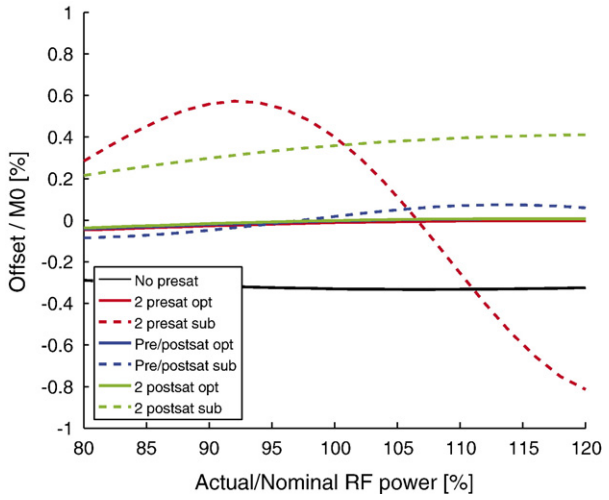

Fig. 5. Effect of B_1 inhomogeneity. Calculated offset of M_0 (in percentage) is shown as a function of B_1 amplitude (RF power) in a PICORE experiment for different number and placement of presaturation pulses. The results of using both optimal (opt) and suboptimal (sub) crusher gradient combinations are plotted. Sinc/HS RF pulses were used (Table 2, Simulation 2A).

the first two RF pulses results in a large offset of about 1% of M_0. When using two postsats, a large offset is observed when $A_{post}=0.25\times A_{inv}$ for PICORE and $A_{post}=0.25\times A_{inv}-5$ mT/m · ms for FAIR (A, crusher gradient area; post, first postsaturation pulse; inv, inversion pulse). Furthermore, it is seen that for presat/postsat, using a crusher gradient resulting in less than 20 phase rolls over the imaging slab after the inversion pulse results in a large offset regardless of the crusher gradient area after the presat pulse. To avoid a large offset, the difference between successive crusher gradient areas should be ~30% in PICORE experiments and ~50% in FAIR experiments.

The simulation was also run with a tag gap of 37% of the imaging slab (10 mm) using PICORE (not shown), and the results were similar although the offset was smaller.

3.1.2. Simulation 2

Fig. 2 shows the calculated offset for three combinations of RF pulses for the case of two presats and a tag gap of 18.5% of the imaging slab (5 mm). The offset is plotted as a function of the crusher gradient areas. A large offset is seen when the crusher areas in the sinc/HS and SLR/HS simulations are equal, while a very small offset is observed at other combinations. When using sinc/FOCI in the PICORE experiment, there is almost no offset regardless of the size of the crushers. In the FAIR simulation, the offset is large when the second presat crusher gradient area is 7 mT/m · ms lower than the second presat crusher. The simulations for two postsats and presat/postsat showed similar results for the sinc/HS and SLR/HS experiments. Another simulation using presat and postsat (data not shown) showed an offset of up to 8% of M_0 using sinc/FOCI for small presat crusher areas when using either PICORE or FAIR labeling. This offset was independent of the area of the crusher gradient following the inversion pulse.

3.1.3. Simulation 3

Fig. 3 shows the results of Simulation 3. The figure plots the calculated offset as a function of tag gap/inversion slab thickness ratio for different presaturation schemes. It is clearly seen that the offset is reduced by presaturation. For PICORE, it can be further reduced by using multiple presaturation pulses. For FAIR, the use of multiple presaturation pulses does not result in a reduction in the offset compared with the use of one presaturation pulse.

3.1.4. Simulation 4

Fig. 4 shows the effect of using different RF pulses on the offset as a function of tag gap/inversion slab thickness. Panels A and C show the offset when using optimal crusher gradient areas, while Panels B and D show it for suboptimal crusher gradient areas. Optimal crusher gradient areas are defined as combinations of crusher gradient areas giving a minimal offset in Fig. 2, while suboptimal crusher gradient areas are combinations giving a large offset. There is little difference in the observed offset between the RF pulses when using optimal presaturation while there is a large difference when using suboptimal crusher gradient areas. The FOCI inversion pulse is less sensitive to suboptimal crusher areas than the other combinations in the PICORE experiment, while it is very sensitive to suboptimal crusher areas in the FAIR experiment. In the FAIR experiment using optimized presaturation, all RF pulse combinations show a slight offset, which will not be detectable in vivo.

3.1.5. Simulation 5

Fig. 5 shows the offset of M_0 (in percentage) as a function of B_1 amplitude for different positions of the

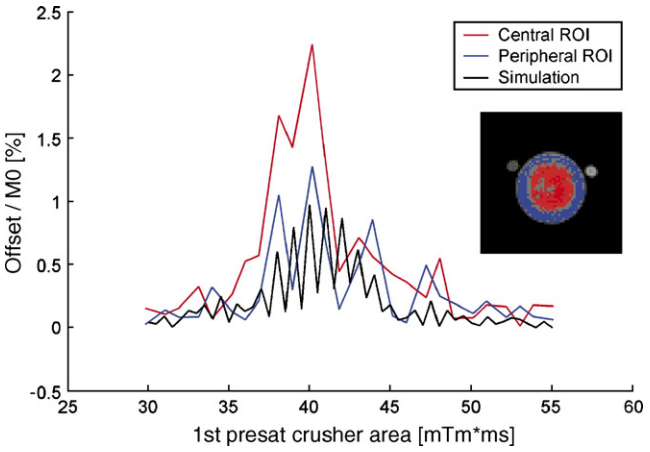

Fig. 6. Verification of simulation results. Offset relative to M_0 as a function of the presat crusher area in a PICORE experiment with two presats. The insert shows the two different ROIs used overlaid on the phantom. The range of crusher gradients used is illustrated as a red line in the top left panel of Fig. 1.

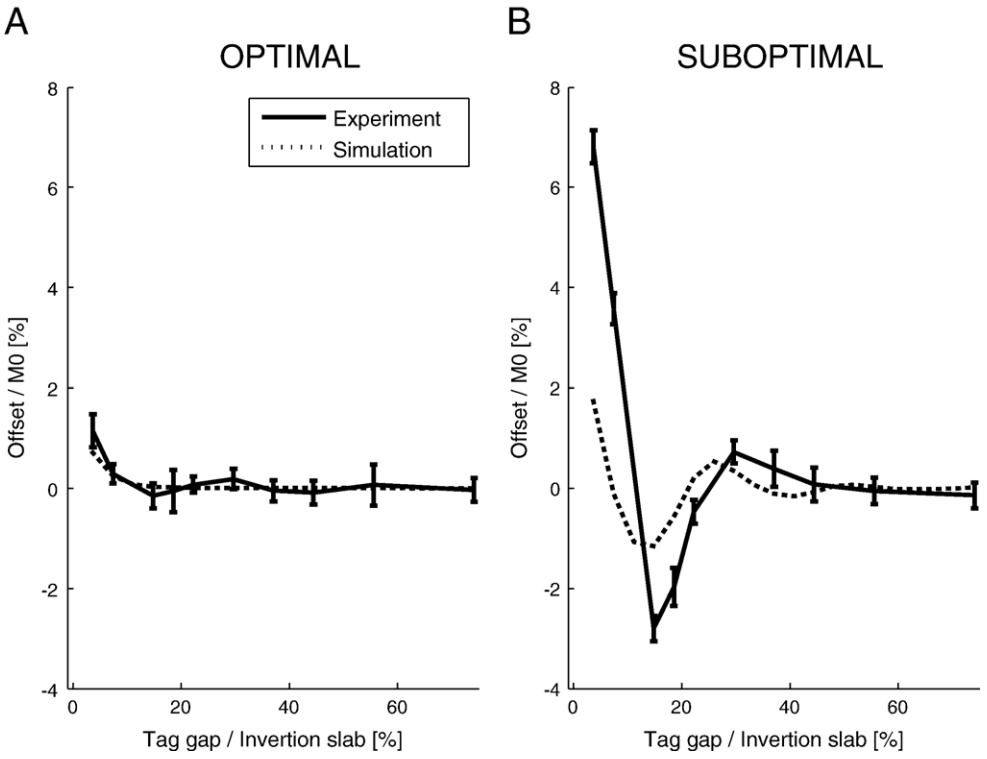

Fig. 7. Offset versus tag gap. Measured and simulated offset relative to M_0 as a function of tag gap. Panel A shows the results for optimal crusher gradient area combinations, while Panel B shows the results for suboptimal combinations (see Table 3, Simulation 3A). Error bars show S.E.M. within the ROIs.

presaturation pulses, as well as for different crusher gradient area combinations, in a PICORE experiment with RF pulses, as shown in Table 2 (Simulation 2A). It is clear that the use of two presat pulses with suboptimal crusher areas results in a large B_1-dependent offset. The B_1 dependence of the offset is diminished for optimal crusher gradient area combinations. The other RF pulse combinations shown in Table 2 were also simulated. When using SLR pulses for presaturation and imaging, the offset was close to zero and constant across B_1 amplitudes except for the suboptimal crusher areas in the simulation with two presats where it was 0.25% at most. When using the FOCI pulse for inversion, all pulses had offsets below 0.02% regardless what the B_1 amplitude was; however, the suboptimal crusher area combinations still showed a slightly larger offset than the optimal ones.

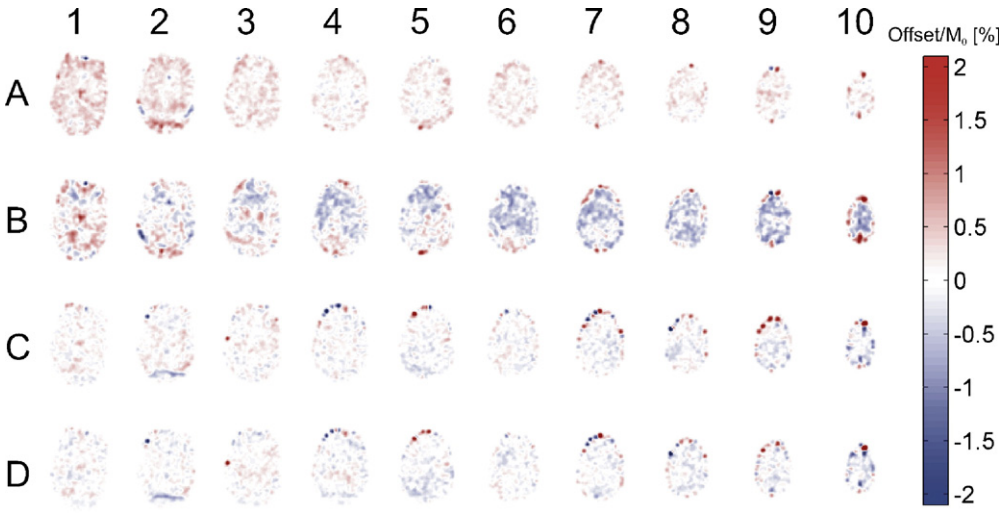

Fig. 8. Difference between images acquired with optimal/suboptimal crusher gradient area combinations and reference image (i.e., the offset) divided by M_0 as a function of slice number for a PICORE experiment with presat/postsat. A: Optimal crusher; tag gap, 9% of the imaging slab. B: Suboptimal crushers; tag gap, 9%. C: Optimal crushers; tag gap, 18%. D: Suboptimal crushers; tag gap, 18% (see Table 3).

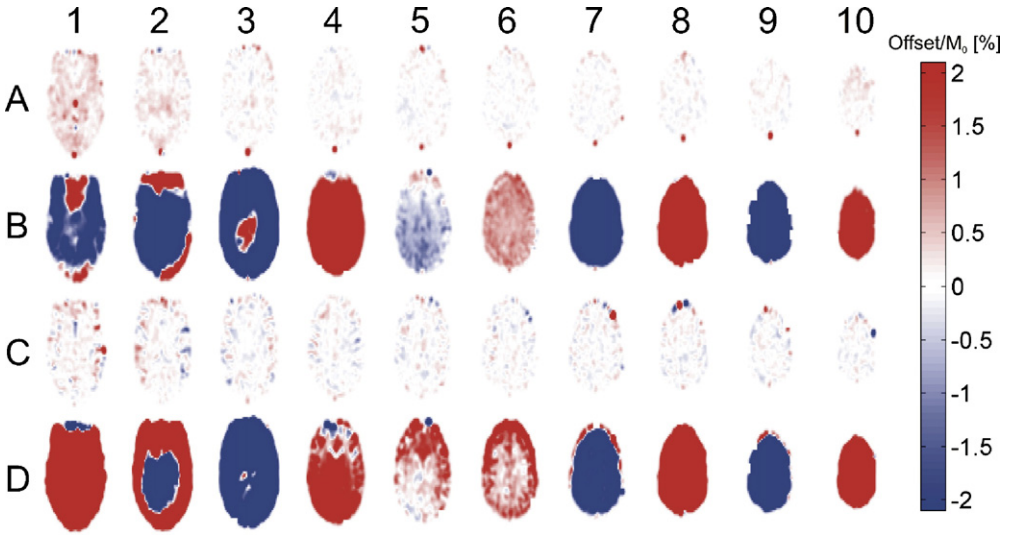

Fig. 9. Difference between images acquired with optimal/suboptimal crusher areas and reference image (i.e., the offset) divided by M_0 as a function of slice number for a FAIR experiment with presat/postsat. A: Optimal crusher; inversion width, 118% of the imaging slab. B: Suboptimal crushers; inversion width, 118%. C: Optimal crushers; inversion width, 137%. D: Suboptimal crushers; inversion width, 137% (see Table 4).

3.2. Phantom and In Vivo Experiments

3.2.1. Phantom Experiment 1

Fig. 6 shows the offset relative to M_0 averaged over two ROIs as a function of the first presat crusher gradient area in a PICORE experiment with two presats (ROIs shown in the insert). The range of crusher gradient areas is illustrated as a profile in Fig. 1. These results confirm that the simulations (black curve) and phantom experiments (red and blue curve) are in agreement. They also show that the offset between the tag and control image is different in the central and peripheral parts of the phantom. This confirms the B_1 dependence of the offset when using suboptimal crusher gradient area combinations found in Simulation 5.

3.2.2. Phantom Experiment 2

Fig. 7 shows both the measured (from the central ROI) and simulated offsets relative to M_0 as a function of the tag gap in a PICORE experiment with two presats. The offset is lower for optimal crusher gradient area combinations than for suboptimal combinations for tag gaps less than 50% of the imaging slab. The figure also shows good agreement between simulations and phantom experiments.

3.2.3. In Vivo Experiment 1

Fig. 8 shows the offset measured in vivo in a typical subject using a PICORE sequence with presat/postsat for both optimal and suboptimal crusher gradient area combinations as well as two different tag gaps. It is seen that the optimal crusher gradient combinations give a small positive offset at 9% tag gap in the inferior slices (A), while the suboptimal crusher gradient area combinations give a negative offset in the superior slices (B). At a gap of 18%, the optimal and suboptimal crusher gradient area combinations give similar results and the difference between the measured images and the reference is very small.

Fig. 9 shows the offset measured in vivo in a typical subject using a FAIR sequence with presat/postsat for both optimal and suboptimal crusher gradient area combinations as well as two different tag gaps. It is clear from the figure that in the FAIR experiment, the perfusion images are very different for the optimal and suboptimal crusher gradient area combinations where a very large offset is seen when using suboptimal gradient area combinations. This offset even oscillates in sign over slices.

Table 5 lists the mean offset and standard deviation over subjects in the posterior gray matter ROI. Results for the other ROIs were similar.

As seen in the table, almost all experiments using presaturation (5B–E) were significantly different from experiments with no presat (5A) except for the presat/postsat FAIR experiment (5D).

None of the experiments showed a significant difference between the use of optimal and suboptimal crusher areas when using multiple presaturation pulses. The FAIR experiment using suboptimal crushers and presat/postsat (5D) shows a large offset (2.1% of M_0) that is not signi-

Table 5
Offset relative to M_0 (%) between perfusion-weighted images and reference image for different presaturation schemes as well as both optimal and suboptimal crusher gradient area combinations

Experiment	PICORE		FAIR	
	Optimal	Suboptimal	Optimal	Suboptimal
5A, no presat	1.2 (0.15)	N/A	0.5 (0.14)	N/A
5B, 1 presat	0.8 (0.28)*	N/A	0.3 (0.16)*	N/A
5C, 2 presats	0.4 (0.08)*	0.5 (0.22)*	0.2 (0.18)†	0.3 (0.18)*
5D, presat/postsat	0.4 (0.11)*	0.3 (0.08)*	0.3 (0.10)	2.1 (1.35)
5E, 2 postsats	0.4 (0.08)†	0.6 (0.39)†	0.2 (0.11)*	0.2 (0.08)*

Data are averages (S.D.) from four subjects.
* Significantly different from no presat (5A; $P<.05$).
† Significantly different from 1 presat (5B) and no presat (5A; $P<.05$).

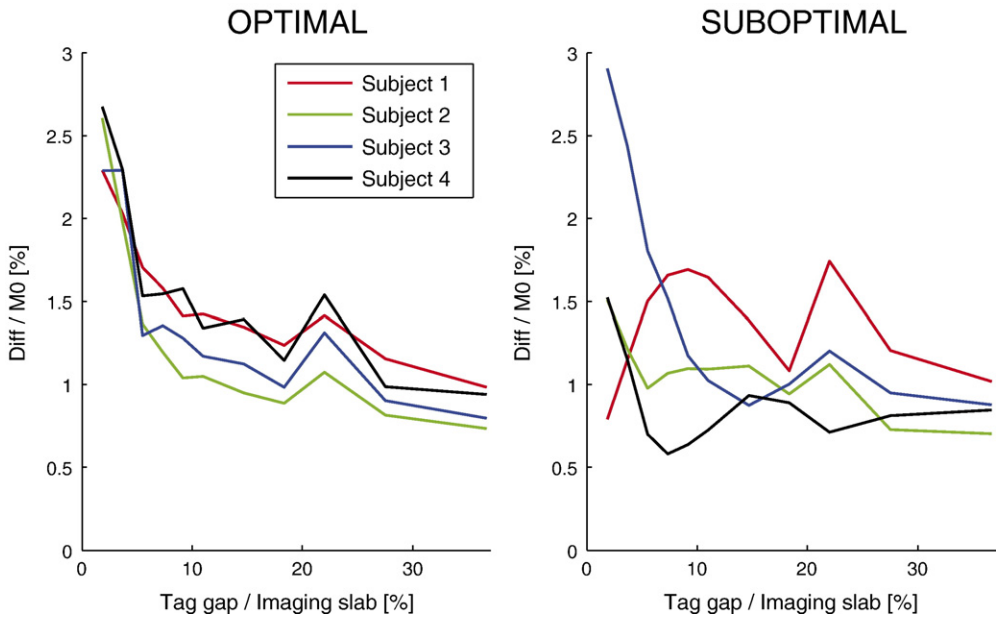

Fig. 10. Effect of using optimal crusher areas in vivo. Difference signal relative to M_0 for different tag gaps in a posterior gray matter ROI. The offset is plotted for each subject scanned using optimal crusher gradient area combinations (left) and suboptimal crusher gradient area combinations (right).

ficantly different from using no presat or one presat. This is caused by the large S.D. between subjects (1.35%), which is because the offset is different for a given slice across subjects.

3.2.4. In Vivo Experiment 2

The results of this experiment are shown in Fig. 10 where the measured ASL difference signal averaged over a posterior gray matter ROI is plotted as a function of tag gap. Panel A shows the results using optimal crusher gradient area combinations, while Panel B shows them for suboptimal combinations. The results were similar in the rest of the ROIs except that the perfusion signal was lower in the white matter than the gray matter. In Panel A, the perfusion signal decreases as a function of tag gap, which is expected as the increase in tag gap will result in an increased transit time, resulting in less inverted blood reaching the imaging area when the tag gap is increased. A small peak is seen at a 22% tag gap (12 mm), which was not seen in the phantom experiments. The suboptimal crusher gradient area combination experiment shows large fluctuations in the signal over subjects, in agreement with higher B_1 sensitivity for suboptimal crushers. Subject 3, however, shows results that are quite similar to the results obtained using optimal crusher gradient area combinations.

4. Discussion

4.1. Presaturation

This study has confirmed that presaturation in ASL experiments may lead to improved static tissue subtraction compared with experiments without presaturation. Furthermore, it has been found that the use of multiple saturation pulses, each followed by crusher gradients, can enhance the effect of presaturation (especially two postsats for PICORE and two presats for FAIR) but may also result in large offsets between the tag and control image that are not perfusion related (Fig. 1). These offsets are caused by unwanted refocused coherence pathways (stimulated echoes). The offset is particularly large if the first two successive crusher gradients have equal areas in experiments using two presats or prestat/postsat.

Poor selection of presaturation crusher gradient areas can lead to large offsets (Fig. 9 and Table 5, Experiment 5D). The PICORE experiment shows a larger difference between the reference image and the 9% tag gap than the reference image and the 18% tag gap (Fig. 8). This is most likely caused by more labeled blood reaching the imaging slab as a result of the reduced transit time.

In vivo, it was shown that the use of presaturation pulses could reduce the offset in almost all experiments. Using multiple presaturation pulses appears to reduce the offset (Table 5). However, with the number of subjects investigated here, there was only a significant difference between using one presat and multiple presaturation pulses for two postsats in PICORE and two presats in FAIR.

4.2. Changing the position of the presaturation pulses

Changing the position of the presaturation pulses has an effect on which crusher area combination should be avoided (Fig. 1). However, if the crusher areas are selected carefully, there is not much resultant difference. This was further confirmed in Fig. 3, which shows that changing the position of the presaturation pulses does not significantly reduce the

minimum tag gap in either FAIR or PICORE. However, multiple presaturation pulses do reduce the minimum tag gap in the simulations.

4.3. Specialized RF pulses

When using optimized inversion and imaging RF pulses, the use of multiple presaturation pulses can still cause a large offset if the crusher areas are selected poorly as shown in Fig. 2. However, in a PICORE simulation using sinc/FOCI, the offset is very small regardless of the choice of crusher gradient areas. These results were confirmed in a simulation comparing the use of optimal and suboptimal crusher areas while stepping the tag gap (Fig. 4).

A study by Yongbi et al. [6] has shown that the necessary inversion width in a FAIR experiment was 240% and 130% of the imaging slab for HS inversion and c-FOCI inversion, respectively. Our simulations suggest that the necessary inversion width can be reduced to 122% of the imaging slab when using standard HS inversion pulses combined with optimal presaturation in a FAIR experiment.

4.4. B_1 inhomogeneity

The offset between the tag and control image was shown to vary with the size of B_1 (Figs. 5 and 6). When using suboptimal crusher areas, the offset is up to 0.5% of M_0, which is on the order of the perfusion signal. As B_1 inhomogeneity increases with field strength, this error is expected to be worse in high-field MR systems.

Depending on the used RF coil, B_1 amplitude can vary with position, and as the offset also varies with B_1 amplitude, this can lead to spatially dependent errors in the measured perfusion images. The use of optimal crusher areas, however, reduces this sensitivity, which is in agreement with previous findings [11].

4.5. Validity of offset estimation in vivo

It is difficult to estimate how much of the difference between the tag and control images in vivo comes from perfusion and how much comes from the non-perfusion-related offset. In this study, we used subtraction of a reference scan to give an estimate of the offset. However, with increasing tag gap, the transit delay (time from labeling until the blood reaches the imaging slab) will also increase, which means that the perfusion-related signal will be different for different tag gaps. However, as seen in Fig. 10, the offset versus tag gap curve has a very quick descending component, as well as a slowly decreasing component. The slow decrease is most likely caused by differences in transit time, while the fast decrease can be attributed to non-perfusion-related differences (offsets).

An alternative approach for estimating the offset would be to inject Gd-DTPA, which reduces the T_1 value of blood. This causes rapid relaxation of the arterial tag during the transit time and eliminates most of the perfusion signal [6]. Due to the invasive nature of this approach, it was not used in this study.

4.6. Effect in vivo

Reducing the gap between the inversion and imaging area minimizes the transit times and results in an increase in the perfusion signal. A decrease in transit time not only increases the amount of tagged blood that has reached the imaging slice but also allows for shorter inversion times, which increases the signal as the tagged blood bolus will have undergone less T_1 relaxation.

This is important if quantitative imaging of perfusion using a single subtraction (QUIPSS) II [12] is used to acquire quantitative images, as one of the requirements for QUIPSS II is that TI_2 must be larger than the sum of TI_1 and the transit time.

It could also be important in clinical scanners with low field strength and in ASL functional MRI (fMRI). A previous study has shown that reducing this gap from 10 to 5 mm more than doubles the number of significantly activated pixels in ASL fMRI [13]. In the previous study, the reduction of the gap was made possible by estimating the offset caused by incomplete static tissue subtraction. In this study, static tissue subtraction was improved by the use of multiple saturation pulses.

5. Conclusion

Using simulations as well as phantom and in vivo studies, we demonstrate in this work that optimization of presaturation can be used to minimize the required gap between inversion and imaging slabs in pulsed ASL experiments, which can lead to significant increases in sensitivity. Minimizing the gap is especially important in fMRI studies where sensitivity is a critical issue.

This study has shown that the gap between inversion and imaging slabs using PICORE can be reduced to 15% of the imaging slab. In FAIR, the inversion slab can be reduced to 122% of the imaging slab. However, care must also be taken when using multiple saturation pulses since poor selection of crusher gradient areas can lead to large non-perfusion-related offsets. It was also shown that the use of optimal saturation and inversion with sinc and HS RF pulses can give equally good static tissue subtraction as the use of FOCI inversion RF pulses or SLR saturation and imaging RF pulses.

Acknowledgments

The authors thank the Technical University of Denmark, the Danish Research Centre for Magnetic Resonance and the Graduate School for Biomedical Optics and New Laser Systems for funding and Ian Rowland for assistance in preparing the manuscript.

References

[1] Wong EC, Buxton RB, Frank LR. Implementation of quantitative perfusion imaging techniques for functional brain mapping

using pulsed arterial spin labeling. NMR Biomed 1997;10(4–5): 237–49.

[2] Kim SG. Quantification of relative cerebral blood flow change by flow-sensitive alternating inversion recovery (FAIR) technique: application to functional mapping. Magn Reson Med 1995;34(3):293–301.

[3] Barbier EL, Lamalle L, Decorps M. Methodology of brain perfusion imaging. J Magn Reson Imaging 2001;13(4):496–520.

[4] Frank LR, Wong EC, Buxton RB. Slice profile effects in adiabatic inversion: application to multislice perfusion imaging. Magn Reson Med 1997;38(4):558–64.

[5] Keilholz-George SD, Knight-Scott J, Berr SS. Theoretical analysis of the effect of imperfect slice profiles on tagging schemes for pulsed arterial spin labeling MRI. Magn Reson Med 2001;46(1): 141–8.

[6] Yongbi MN, Yang Y, Frank JA, Duyn JH. Multislice perfusion imaging in human brain using the C-FOCI inversion pulse: comparison with hyperbolic secant. Magn Reson Med 1999;42(6):1098–105.

[7] Yongbi MN, Branch CA, Helpern JA. Perfusion imaging using FOCI RF pulses. Magn Reson Med 1998;40(6):938–43.

[8] Sidaros K, Andersen IK, Liu TT, Wong EC, Buxton RB. The effects of the order of saturation and inversion in pulsed arterial spin labeling. Proceedings of the 11th Annual Meeting of the International Society of Magnetic Resonance in Medicine, 2003. p. 2214.

[9] Silver MS, Joseph RI, Hoult DI. Highly selective pi/2 and pi pulse generation. J Magn Reson 1984;1(59):347–51.

[10] Matson GB. An integrated program for amplitude-modulated RF pulse generation and re-mapping with shaped gradients. Magn Reson Imaging 1994;12(8):1205–25.

[11] Sidaros K, Andersen IK, Liu TT, Wong EC, Buxton RB. Presaturation efficiency in pulsed arterial spin labeling in the presence of B1 inhomogeneities. Proceedings Eleventh ISMRM, 2003. p. 2214.

[12] Wong EC, Buxton RB, Frank LR. Quantitative imaging of perfusion using a single subtraction (QUIPSS and QUIPSS II). Magn Reson Med 1998;39(5):702–8.

[13] Sidaros K, Liu TT, Lund TE, Wong EC, Buxton RB. Improved SNR in perfusion fMRI by offset correction. Proceedings of the 10th Annual Meeting of the International Society of Magnetic Resonance in Medicine, 2002. p. 624.

[14] Ordidge RJ, Wylezinska M, Hugg JW, Butterworth E, Franconi F. Frequency offset corrected inversion (FOCI) pulses for use in localized spectroscopy. Magn Reson Med 1996;36(4):562–6.

[15] Shinnar M, Boliger L, Leigh JS. Synthesis of soft pulses with specified frequency responses. Proceedings 7th SMRM, 1988. p. 1040.

[16] Le Roux P. Exact synthesis of radio frequency waveforms. Proceedings 7th SMRM, 1988. p. 1049.